AD-A147 385 A 'HYDROGEN PARTITIONING' MODEL FOR HYDROGEN ASSISTED CRACK GROWTH(U) LEHIGH UNIV BETHLEHEM PA INST OF FRACTURE AND SOLID MECHANICS M GAO ET AL. SEP 84 1/1

UNCLASSIFIED IFSM-84-127 N00014-83-K-0107 F/G 20/11 NL

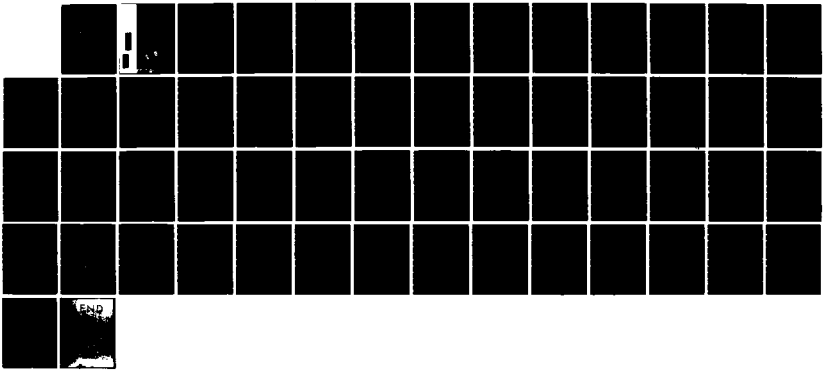

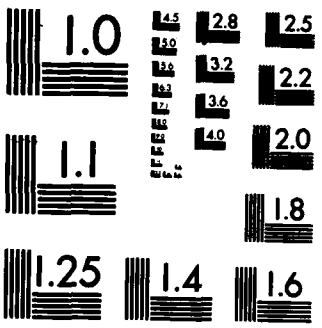
1.0
1.1
1.25
1.4
1.6
1.8
2.0
2.2
2.5
2.8
3.2
3.6
4.0
4.5
5.0
5.6
6.3
7.1

DTIC FILE COPY
AD-A147 385
LEHIGH UNIVERSITY - INSTITUTE FOR FRACTURE AND SOLID MECHANICS

(12)

IFSM 84-127

LEHIGH UNIVERSITY

A "HYDROGEN PARTITIONING" MODEL FOR HYDROGEN ASSISTED CRACK GROWTH

by

M. Gao and R. P. Wei

DTIC ELECTE NOV 13 1984 S E D

September, 1984

Technical Report No. 17
Office of Naval Research
Contract N00014-83-K-0107, NR 036-097

This document has been approved for public release and sale; its distribution is unlimited.

84 11 06 268

A "HYDROGEN PARTITIONING" MODEL FOR HYDROGEN ASSISTED CRACK GROWTH

by

M. Gao[1] and R. P. Wei[2]
Lehigh University
Bethlehem, PA 18015

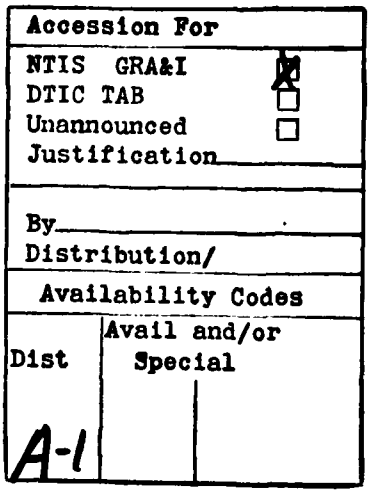

Technical Report No. 17

OFFICE OF NAVAL RESEARCH

This document has been approved for public release and sale; its distribution is unlimited.

[1]Visiting Scholar. Now Associate Professor, Department of Materials Sciences, Shanghai Jiao Tong University, Shanghai, People's Republic of China.

[2]Professor, Department of Mechanical Engineering and Mechanics.

Unclassified
SECURITY CLASSIFICATION OF THIS PAGE (When Date Entered)

REPORT DOCUMENTATION PAGE	READ INSTRUCTIONS BEFORE COMPLETING FORM
1. REPORT NUMBER: IFSM-84-127 ✓ 2. GOVT ACCESSION NO.: AD-A147385	3. RECIPIENT'S CATALOG NUMBER
4. TITLE (and Subtitle): A "HYDROGEN PARTITIONING" MODEL FOR HYDROGEN ASSISTED CRACK GROWTH	5. TYPE OF REPORT & PERIOD COVERED: Technical Report No. 17
	6. PERFORMING ORG. REPORT NUMBER
7. AUTHOR(s): M. Gao and R. P. Wei	8. CONTRACT OR GRANT NUMBER(s): Contract N00014-83-K-0107
9. PERFORMING ORGANIZATION NAME AND ADDRESS: Lehigh University, Bethlehem, PA 18015	10. PROGRAM ELEMENT, PROJECT, TASK AREA & WORK UNIT NUMBERS: NR 036-097
11. CONTROLLING OFFICE NAME AND ADDRESS: Office of Naval Research, Department of the Navy, Arlington, VA	12. REPORT DATE: September, 1984
	13. NUMBER OF PAGES: 54
14. MONITORING AGENCY NAME & ADDRESS(if different from Controlling Office)	15. SECURITY CLASS. (of this report): Unclassified
	15a. DECLASSIFICATION/DOWNGRADING SCHEDULE

16. DISTRIBUTION STATEMENT (of this Report)

This document has been approved for public release and sale; its distribution is unlimited.

17. DISTRIBUTION STATEMENT (of the abstract entered in Block 20, if different from Report)

18. SUPPLEMENTARY NOTES

19. KEY WORDS (Continue on reverse side if necessary and identify by block number)

Hydrogen, partitioning, microstructure, steels, hydrogen embrittlement, fracture mechanics

20. ABSTRACT (Continue on reverse side if necessary and identify by block number)

A "hydrogen partitioning" model has been developed to account for the pressure and temperature dependence for hydrogen-assisted crack growth. The model gives explicit recognition to the role of hydrogen-microstructure interactions in determining the distribution (or partitioning) of hydrogen among the various microstructural elements (principally between the prior-austenite grain boundaries and the matrix) and the rate of crack growth along the

DD FORM 1 JAN 73 1473 EDITION OF 1 NOV 65 IS OBSOLETE
S/N 0102-014-6601

Unclassified
SECURITY CLASSIFICATION OF THIS PAGE (When Date Entered)

elements. It also takes into account the role of various rate controlling processes in determining the rate that hydrogen is being supplied to the fracture process (or embrittlement) zone.

Quantitative assessment of the model indicates very good agreements between the model predictions and the observed crack growth responses for AISI 4340 and 4130 steels tested in hydrogen and for AISI 4340 steel tested in hydrogen sulfide. This model accurately characterizes the reduction in crack growth rate and the concomitant change in fracture mode at "high" temperatures. Through its integration with the earlier models, based on rate controlling processes, the model predicts the pressure and temperature dependence for K-independent crack growth over the entire range of environmental conditions.

A "HYDROGEN PARTITIONING" MODEL FOR HYDROGEN ASSISTED CRACK GROWTH

M. Gao[1/] and R. P. Wei[2/]
Lehigh University
Bethlehem, PA 18015

ABSTRACT

A "hydrogen partitioning" model has been developed to account for the pressure and temperature dependence for hydrogen-assisted crack growth. The model gives explicit recognition to the role of hydrogen-microstructure interactions in determining the distribution (or partitioning) of hydrogen among the various microstructural elements (principally between the prior-austenite grain boundaries and the matrix) and the rate of crack growth along the elements. It also takes into account the role of various rate controlling processes in determining the rate that hydrogen is being supplied to the fracture process (or embrittlement) zone.

Quantitative assessment of the model indicates very good agreements between the model predictions and the observed crack growth responses for AISI 4340 and 4130 steels tested in hydrogen and for AISI 4340 steel tested in hydrogen sulfide. This model accurately characterizes the reduction in crack growth rate and the concomitant change in fracture mode at "high' temperatures. Through its integration with the earlier models, based on rate controlling processes, the model predicts the pressure and temperature dependence for K-independent crack growth over the entire range of environmental conditions.

1/ Visiting Scholar. Now Associate Professor, Department of Materials Sciences, Shanghai Jiao Tong University, Shanghai, People's Republic of China.

2/ Professor, Department of Mechanical Engineering and Mechanics.

1. INTRODUCTION

Subcritical crack growth in high strength steels exposed to gaseous environments has been widely studied from an interdisciplinary point of view. A series of parallel fracture mechanics and surface chemistry studies on AISI 4130 and 4340 steels, exposed to hydrogen containing gases (such as, hydrogen, hydrogen sulfide and water vapor) and to water, have provided a fair understanding of environmentally assisted crack growth [1-11].

It is now clear that environmentally assisted crack growth is controlled by a number of processes in the embrittlement sequence [4]. The various processes that might be involved are (i) transport of the gas or gases to the crack tip, (ii) the reactions of the gas or gases with newly created crack surfaces to evolve hydrogen (viz., physical and dissociative chemical absorption in sequence), (iii) hydrogen entry (or absorption), (iv) diffusion of hydrogen to the fracture (or embrittlement) sites, and (v) hydrogen-metal interactions leading to embrittlement (i.e., the embrittlement reaction), see Fig. 1. According to the multi-reaction rate theory [12], the overall crack growth response is governed by the slowest unit process in the chain of processes operating in sequence. Any one of these processes may act as the rate-controlling process, depending on the environment-material condition (material, environment, pressure, temperature, etc.).

For AISI 4130 and 4340 steels exposed to hydrogen [1-3, 6-8] and hydrogen sulfide [9], the K-independent Stage II crack growth exhibits substantially different responses in two temperature regions, Fig. 2. At "low" temperatures, crack growth reflects control by gas transport to

the crack tip (hydrogen sulfide at the lower pressure, curve b), by surface reaction (hydrogen or water, curves c and d), and by hydrogen diffusion (hydrogen sulfide at the higher pressure, curve a). The crack growth rates conform to the temperature and pressure dependence of the rate controlling process [11]. At "high temperatures", the growth rates are substantially lower than those given by these processes, and some other process appears to be in control. The intermediate region (Region B) represents the transition between Regions A and C. The fundamental question posed by these results is which process or processes cause the decrease in crack growth rate at "high temperatures".

Attempts to explain this behavior were first made by Williams, Nelson and Tetelman [1-3] in the early 1970's. According to their surface reaction model, the high temperature region of crack growth response is controlled by the equilibrium between absorbed hydrogen and gaseous hydrogen. Subsequently, several "surface reaction" models were proposed by other researchers [13-15]. These models are purely chemical and considered only surface reactions in controlling crack growth response even though other processes might have been in control (Fig. 2) [9-11].

Recent fractographic studies on an AISI 4340 steel indicated that the reduction in crack growth rate with increasing temperature into the high temperature region is accompanied by a change in fracture surface morphology; namely, from intergranular to transgranular (micro-void coalescence type) failure [16]. This finding implied that the associated change in hydrogen supply (as predicted by the surface reaction models) could not be the sole cause for the observed change in crack growth response. The observed difference in fracture surface morphology

suggested that different micromechanisms or different hydrogen embrittlement processes might be in control for the two temperature regions.

To clarify this issue, the response of different microstructural elements to hydrogen embrittlement and the partitioning of hydrogen among these elements as a function of temperature and pressure are considered. A "hydrogen partitioning" model for crack growth in gaseous environments is proposed. The model provides a direct correlation of crack growth kinetics with the response of microstructural elements to hydrogen embrittlement.

2. EXPERIMENTAL BASIS FOR THE MODEL

The proposed model is based on the following experimental findings [16]:

(i) In the low temperature region, the fracture surface morphology is characterized by intergranular separation along prior-austenite grain boundaries, with a small amount of transgranular quasi-cleavage [2,3,17,18]. The fracture mode is unaffected by the rate controlling process for crack growth as long as an adequate amount of hydrogen is supplied.

(ii) The change in Stage II crack growth rate in going from low to high temperature, with a maximum rate at an intermediate temperature, is related to a transition from intergranular and quasi-cleavage to microvoid coalescence modes of separation.

(iii) The temperature at which the transition in fracture surface morphology occurs is dependent on hydrogen and hydrogen sulfide pressure. The higher the gas pressure, the higher is this temperature. This trend is consistent with the effect of gas pressure on the change in crack growth response from low to high temperatures.

These fractographic observations are difficult to explain in terms of the models proposed by Williams and Nelson et al. [1-3, 13-15]. The observed difference in fracture surface morphology and the associated reduction in crack growth rates suggest that different micromechanisms or different hydrogen embrittlement processes need to be considered for the two temperature regions.

To examine the role of micromechanism, one might divide the embrittlement sequence roughly into three portions [16]. These three portions are depicted schematically in Fig. 3. The first portion is concerned with the supply of hydrogen, and includes gas-phase transport (i.e., external transport), surface reactions, and diffusion (i.e., internal transport) of hydrogen to the embrittlement sites. The second portion involves the partitioning of hydrogen among the potential fracture sites in the microstructure. These sites, in AISI 4340 steel, include: (i) the prior-austenite grain boundaries, (ii) the martensite lath or patch boundaries, and $\{110\}_{\alpha'}$ and $\{112\}_{\alpha'}$ planes through the martensites, and (iii) the martensite lattice itself. The third portion deals with the embrittlement reaction at each type of sites, with the prior-austenite grain boundaries being most susceptible and the martensite lattice least susceptible to hydrogen embrittlement.

Cracking at the respective microstructural elements would depend on the concentration and rate of supply of hydrogen there. The overall crack growth rate would be determined by the rates of cracking through the participating microstructural elements.

It is reasonable to suggest that the partitioning or distribution of hydrogen to the different microstructural elements is a function of temperature and pressure. Hence, the concentration and the rate of hydrogen supplied to the different fracture sites become functions of temperature and pressure. At low temperature (Region A), the prior-austenite grain boundaries and the slip planes are saturated by hydrogen. The fracture is therefore predominantly intergranular, and includes a small amount of quasi-cleavage. Because the rate of supply of hydrogen from the external environment is relatively slow, crack growth is controlled by one of the hydrogen supply processes [10,11]. At the higher temperatures, or Region C, the hydrogen concentration at grain boundaries and slip planes is expected to drop quickly and more hydrogen goes into the martensite lattice. Increasing amounts of microvoid coalescence or dimpled failure now occur with increased temperature and result in slower crack growth rates. Accordingly, the changes in crack growth rate and crack growth response with temperature are attributed now to the transfer of micromechanisms of fracture, instead of the processes of hydrogen supply. These considerations are equally applicable to hydrogen and hydrogen sulfide.

3. ASSUMPTIONS AND BASIC EQUATIONS

In developing the model, the following five assumptions are made:

(i) Crack growth is at steady state, and is in Stage II. Hence, the crack growth rate remains constant at a given temperature and hydrogen pressure, and is independent of the stress intensity factor K.

(ii) The rate of hydrogen supplied to the fracture process zone is governed by the controlling process for hydrogen supply. These processes include (a) transport of the deleterious gas to the crack tip, (b) surface reaction of the gas with the newly created surface at the crack tip, and (c) diffusion of hydrogen to the embrittlement region ahead of the crack tip.

(iii) The controlling process of hydrogen supply remains unchanged over the range of temperature of interest; that is, from Region A to Region C.

(iv) The rate of crack growth for each fracture mode is determined by the rate of supply of hydrogen to each type of fracture site, $\dot{Q}_i$.

(v) The different micromechanisms of cracking operate in parallel or concurrently.

Based on these assumptions, the crack growth rate for the i^{th} fracture mode (or micromechanism), $(da/dt)_i$, is given by Eqn. (1). In the equation, α_i is the proportionality constant for the i^{th} mode.

$$(da/dt)_i = \alpha_i \dot{Q}_i \tag{1}$$

For concurrent growth, the mean crack growth rate, $(da/dt)_{II}$ is the sum of the products of growth rate and the corresponding areal fraction, f_i, of the individual modes on the fracture surface, and is given by Eqn. (2).

$$(da/dt)_{II} = \sum_i f_i \alpha_i \dot{Q}_i \tag{2}$$

For AISI 4340 steel fractured in hydrogen and hydrogen sulfide, the areal fraction of quasi-cleavage (f_q) is small (less than about 14%) as compared with that of grain boundary separation at low temperatures, and is nearly zero at the higher temperatures [16]. The contribution of quasi-cleavage to the main crack growth rate, therefore, may be neglected. Then, Eqn. (2) can be simplified as follows:

$$\begin{aligned}(da/dt)_{II} &\approx f_b \alpha_b \dot{Q}_b + f_\ell \alpha_\ell \dot{Q}_\ell \\ &= (f_b \alpha_b \kappa_b + f_\ell \alpha_\ell \kappa_\ell)\dot{Q}\end{aligned} \tag{3}$$

where $\dot{Q}$ is the total rate of hydrogen supplied to fracture process zone, and κ_b, κ_ℓ are the hydrogen distribution coefficients ($\kappa_b = \dot{Q}_b/\dot{Q}$, $\kappa_\ell = \dot{Q}_\ell/\dot{Q}$, and $\kappa_b + \kappa_\ell = 1$).

Equations (2) and (3) are two of the basic equations for the model. For simplicity, only Eqn. (3) is used in further quantification of the model.

4. DISTRIBUTION COEFFICIENTS AND HYDROGEN SUPPLY RATE

4.1 Distribution Coefficients κ_b and κ_ℓ

The distribution coefficients κ_b and κ_ℓ are defined as the fraction of the rate of hydrogen being supplied to the grain boundaries and to the lattice respectively, i.e.:

$$\kappa_b = \dot{Q}_b/\dot{Q} = (\dot{Q}_b/\dot{Q}_\ell)/(1 + \dot{Q}_b/\dot{Q}_\ell) \tag{4.a}$$

$$\kappa_\ell = \dot{Q}_\ell/\dot{Q} = 1/(1 + \dot{Q}_b/\dot{Q}_\ell) \tag{4.b}$$

To estimate these coefficients, hydrogen distribution in a moving frame of reference, with the origin at the crack tip, is considered first. Because crack growth is assumed to be at steady state, with constant speed $(da/dt)_{II}$, the average concentration of hydrogen in the fracture process zone, C_v, is independent of time within this moving frame. The average hydrogen concentration in the grain boundaries (C_b) and in the lattice (C_ℓ) in the same zone are also time independent. The exact location, shape and size of the fracture process zone, however, cannot be specified at the present time. For these estimates, it is sufficient to assume it to be inside a circle of diameter ℓ, with its center at the crack tip, Fig. 4, and to assume that hydrogen is confined within this circle.

It can be readily shown that the rates of hydrogen supply to the fracture process zone, and to the grain boundaries and the lattice within this zone are given by Eqns. (5a) to (5c), respectively:

$$\dot{Q} = C_v B\ell(da/dt)_{II} \tag{5.a}$$

$$\dot{Q}_b = C_b \delta B\ell(da/dt)_{II} \tag{5.b}$$

$$\dot{Q}_\ell = C_\ell(1-\delta)B\ell(da/dt)_{II} \qquad (5.c)$$

In Eqn. (5), δ and $(1-\delta)$ are the volume fractions of prior-austenite grain boundaries and lattice, respectively in the fracture process zone. Hydrogen concentration is given in moles per unit volume. By substituting (5.b) and (5.c) into (4.a) and (4.b), the distribution coefficients become

$$\kappa_b = \frac{[\delta/(1-\delta)](C_b/C_\ell)}{1+[\delta/(1-\delta)](C_b/C_\ell)} \qquad (6.a)$$

$$\kappa_\ell = \frac{1}{1+[\delta/(1-\delta)](C_b/C_\ell)} \qquad (6.b)$$

In general, δ is negligibly small compared with 1. Therefore, Eqn. (6.a) and (6.b) can be further simplified to the following form:

$$\kappa_b = \frac{\delta C_b/C_\ell}{1+\delta C_b/C_\ell} \qquad (7.a)$$

$$\kappa_\ell = \frac{1}{1+\delta C_b/C_\ell} \qquad (7.b)$$

The distribution coefficients (κ_b and κ_ℓ) are now given in terms of the ratio of local concentrations of hydrogen in the grain boundaries and in the lattice, and the volume fraction of grain boundaries.

It is well demonstrated that grain boundaries are strong trapping sites for hydrogen [19-21]. The equilibrium partitioning of hydrogen between the grain boundaries and the lattice can be expressed by either Boltzmann statistics (for dilute solution [22]) or by Fermi-Dirac statistics (for more concentrated solution, or at low temperatures [23]). Even though crack growth is assumed to be at steady state, conditions of equilibrium

may not always be established. Following Bockris [24], therefore, a "non-equilibrium" parameter τ is incorporated in the Boltzmann and the Fermi-Dirac statistics:

$$C_b/C_\ell = \tau(a^3/n)\, N_x \exp\,(H_B/RT) \qquad \text{Boltzmann} \qquad (8.a)$$

$$C_b/C_\ell \simeq \frac{\tau(a^3/n)N_x \exp(H_B/RT)}{1+2(a^3/n)N_A C_\ell \exp(H_B/RT)} \qquad \text{Fermi-Dirac} \qquad (8.b)$$

The parameter τ is equal to 1 when trapping is in equilibrium. N_x is the density of trap sites in the grain boundaries (number of sites/m^3), a is the lattice parameter of the metal, n is the number of atoms per unit cell, N_A is Avogadro constant, and H_B is the binding enthalpy of hydrogen to the grain boundary. Detailed derivation of Eqns. (8.a) and (8.b) is given in Appendix I. Final expressions for κ_b and κ_ℓ can be readily obtained by substituting Eqns. (8.a) and (8.b) into Eqns. (7.a) and (7.b).

It should be noted that either the Boltzmann or the Fermi-Dirac statistics may be used. The choice between these two statistics, however, is not crucial to modeling and quantitative analyses, because both sets give the same values for κ_b and κ_ℓ at low temperatures*. At high temperatures, Boltzmann and Fermi-Dirac statistics themselves are essentially the same. For simplicity, Boltzmann statistics are chosen for use in the present study.

*By examining Eqns. (8.a) and (8.b), it can be seen that $C_b/C_\ell >> 1$ when the temperature is low for both statistics. Substituting k into Eqns. (7.a) and (7.b) gives $\kappa_b = 1$, and a negligibly small value for κ_ℓ.

4.2 Hydrogen Supply Rate $\dot{Q}$

According to assumption (2), the rate of hydrogen supply is controlled by one of the processes for hydrogen supply; with a particular process in control over a given range of pressure and temperature. Using results from recent studies and from modeling of crack growth for each of the controlling processes [4-11, 25], the hydrogen supply rate ($\dot{Q}$), for simplified cases, may be given in the following form:

For transport control (based on Knudsen flow) [9,26]

$$\dot{Q} \propto p_o/T^{\frac{1}{2}} \tag{9.a}$$

For surface reaction control [8, 27]

$$\dot{Q} \propto p_o^m \exp(-E_s/RT) \tag{9.b}$$

For diffusion control [28]

$$\dot{Q} \propto p_o^{\frac{1}{2}} \exp(-E_d/2RT) \tag{9.c}$$

In Eqn. (9), p_o is the external pressure; m is the exponent for pressure dependence for surface reaction; E_s and E_d are the activation energies for surface reaction and for diffusion, respectively; T is the absolute temperature; and R is the gas constant. The precise form of these equations depends on the details of the various processes.

5. FORMULATION OF STAGE II CRACK GROWTH RATE

By incorporating the various parameters into Eqn. (3), the final formulas for Stage II crack growth are obtained.

For transport control

$$(da/dt)_{II} = (\sum_i \alpha_i f_i \kappa_i)\dot{Q}$$

$$= (\sum_i \alpha_i f_i \kappa_i)\eta_t (p_o/T^{\frac{1}{2}}) \qquad (10.a)$$

For surface reaction control

$$(da/dt)_{II} = (\sum_i \alpha_i f_i \kappa_i)\eta_s p_o^{\,m} \exp(-E_s/RT) \qquad (10.b)$$

For diffusion control

$$(da/dt)_{II} = (\sum_i \alpha_i f_i \kappa_i)\eta_d p_o^{\frac{1}{2}} \exp(-E_d/2RT) \qquad (10.c)$$

In the equations, η_t, η_s and η_d are the hydrogen supply rate coefficients for transport control, surface reaction control and diffusion control, respectively. The quantity $(\sum_i \alpha_i f_i \kappa_i)$ is given by Eqn. (11)

$$\sum_i \alpha_i f_i \kappa_i = \left\{ \frac{\alpha_b f_b \tau\delta (a^3/n) N_x \exp(H_B/RT)}{1+\tau\delta (a^3/n) N_x \exp(H_B/RT)} + \frac{\alpha_\ell (1-f_b)}{1+\tau\delta (a^3/n) N_x \exp(H_B/RT)} \right\} \qquad (11)$$

These equations of stage II crack growth rates apply over the entire range of temperatures, from Region A to C, as long as a single process for hydrogen supply is in control. The specific form, again, would depend on the details of the controlling processes. For comparisons with experimental data and for estimating certain parameters, the limiting forms of $(da/dt)_{II}$ are considered.

6. COMPARISON OF THE MODEL TO EXPERIMENTAL DATA

Data on AISI 4340 steel, tested in hydrogen and in hydrogen sulfide [7,9], are used to test the model. Results from the two environments are considered separately in the following subsections.

6.1 Hydrogen

For tests in hydrogen, the rate of hydrogen supply is controlled by the rate of surface reaction [7]. In this case, the crack growth rate is given by Eqn. (10.b). Nearly all of the parameters in this equation are either known or can be estimated from the experimental data. Evaluations of these parameters are described in Appendix II.

The two remaining unknowns are the density of trap sites in the grain boundaries (N_x) and the non-equilibrium parameter (τ). For a given microstructure, N_x must be a constant and ranges from 10^{19} to 10^{23} m^{-3} [23]. The parameter τ, which was introduced into the Boltzmann equation to account for non-equilibrium, may or may not be a constant. If equilibrium is attained, then τ would be constant and is equal to one. In general, however, τ is expected to be a function of temperature and pressure. For now, as an initial effort, τ is assumed to remain constant for a given pressure. The pressure and temperature dependence for τ will be considered further in Section 7.

For the convenience of numerical analyses, an "apparent" density of occupied trap sites in the grain boundaries (N_{app}) is defined, with $N_{app} = \tau N_x$. Since all of the parameters, except N_{app} in Eqn. (10.b) are known, a non-linear least-squares curve fitting program can be used to

search for the value of N_{app} that provides the best fit to the experimental data. The best values of N_{app} obtained are 3.8×10^{22}, 2.88×10^{22} and 8.56×10^{21} m^{-3} for hydrogen pressures of 133, 57 and 13.3 kPa, respectively. Based on these values, corresponding theoretical curves of crack growth over the temperature range, extending from Region A to C, are computed from Eqn. (10.b) and are shown in Fig. 5. These results indicate that the theoretical curves are in good agreement with the experiment. The parameters used in the equation are listed in Table 1. It is interesting to note that the best values of N_{app} are appreciably different for the three different pressures. The "apparent" density of occupied trap sites in the grain boundaries increased with increasing hydrogen pressure. Because N_x is expected to remain constant, this fact clearly indicates that τ is not equal to 1 and that non-equilibrium condition needs to be considered. The physical meaning of τ and N_{app} is discussed in Section 7.

6.2 Hydrogen Sulfide

In the case of hydrogen sulfide, the hydrogen supply rate is controlled by gas transport at low pressure (0.133 kPa) [9]. At a higher pressure (2.66 kPa), the supply rate is controlled by gas transport at intermediate temperatures and by diffusion at the lower temperatures [11, 16]. Hence, in examining the transition from Region A to Region C growth, it is sufficient to consider only the gas transport controlled case for both the low and high pressures. Thus, Eqn. (10.a) is used to predict the crack growth response.

The same values of H_B, a, n, and δ, used for the hydrogen case, are used here, Table 2. The same procedures were used to determine the coefficients and the other parameters. The apparent densities of occupied trap sites, $N_{app} = \tau N_x$, are estimated to be 3.6×10^{22} m^{-3} and 4.2×10^{23} m^{-3} for H_2S pressures of 0.133 kPa and 2.66 kPa, respectively. Again, the predicted curves of crack growth response are in good agreement with the experimental data, as shown in Fig. 6.

7. FURTHER CONSIDERATION OF THE MODEL

7.1 The Physical Meaning of τ

The results given in the previous sections show that (i) the "apparent" density of occupied trap sites at grain boundaries ($N_{app} = 8.5 \times 10^{21}$ to 4.2×10^{23} m^{-3}) is consistent with the range of values that have been proposed for the density of trap sites at grain boundaries (10^{19} to 10^{23} m^{-3}) [23]; (ii) N_{app} varies with pressure, therefore, the parameter τ is not constant and non-equilibrium partitioning of hydrogen between lattice and trap sites should be considered; and (iii) the exact value of τ cannot be determined from N_{app} because N_x is not known.

Originally, Bockris stated that τ could vary from 0 to 1, because filling of the traps with H was achieved by diffusion of hydrogen from the lattice into the trap sites. When equilibrium is not established, then τ must be smaller than 1 [24]. This claim that τ is smaller than one under non-equilibrium conditions, however, may not be always true. When hydrogen enters the material preferentially through the traps, τ can be expected to be greater than one. Here, the establishment of

equilibrium is achieved by the transfer of hydrogen from the trap sites into the lattice. The characteristics of this case may be described as follows:

(i) Hydrogen enters the material directly through the trap sites (such as prior austenite grain boundaries, etc.) and then transfers into the lattice.

(ii) Hydrogen resides at the trap sites and is prevented from diffusing into the lattice. As such, hydrogen concentration could build up preferentially at trap sites and cause τ to become greater than 1. According to Pressouyre and Bernstein, the binding enthalpy to the trap site, H_B>60 kJ/mol dictates irreversibility in hydrogen embrittlement situations [29].

(iii) If hydrogen enters the material predominantly through grain boundaries, then the supersaturability of hydrogen should be proportional to the hydrogen supply rate. Thus, τ, as a measure of supersaturability, may be directly related to the hydrogen supply rate.

From the foregoing discussion, it is believed that the systems which were used to test the model belong to this case. This belief is supported by the following observations:

(i) The crack paths at low temperatures (Region A) is predominantly intergranular. At higher temperatures, specifically in the transition region from A to C, the fracture mode is mixed, but with a major part

by grain boundary separation. These grain boundaries are directly exposed to the environment and are expected to be the preferential paths for hydrogen entry and diffusion.

(ii) The AISI 4340 steel, tempered at 477 K [6], contained a high density of irreversible traps in the form of high angle prior austenite grain boundaries [30]. The binding enthalpy to the grain boundaries has been estimated to be 73 kJ/mol, which satisfies the requirement of binding enthalpy for strong traps.

(iii) The pressure dependence of τ is clearly shown by that of N_{app}. The observed dependence of N_{app} on hydrogen and on hydrogen sulfide pressure (determined to be 0.62 and 0.84 power, respectively) compared well with that for surface reaction controlled process and with that for the transport rate of gases to the crack tip, respectively [25]. These correlations support the earlier assumption that the non-equilibrium parameter τ is proportional to the rate of hydrogen supply to the material.

Thus, instead of assuming τ to be a constant for a given pressure, τ is now assumed to be proportional to the hydrogen supply rate and is given in Eqn. (15).

$$\tau = \begin{cases} \beta_t \eta_t p_o / T^{\frac{1}{2}} & \text{Transport} \quad (12.a) \\ \beta_s \eta_s p_o^{\,m} \exp(-E_s/RT) & \text{Surface Reaction} \quad (12.b) \\ \beta_d \eta_d p_o^{\frac{1}{2}} \exp(-E_d/2RT) & \text{Diffusion} \quad (12.c) \end{cases}$$

where the β's are taken as the proportionality coefficients. This new assumption is used to refine the original model.

7.2 Refinement of the Original Model

Substituting Eqns. (12.a) to (12.c) into Eqns. (10) and (11), a new set of crack growth rate equations are obtained and are as follows:

1) For transport control

$$(da/dt)_{II} = \left\{ \frac{\eta_t^2 \beta_t \alpha_b f_b \delta (a^3/n) N_x (p_o/T^{\frac{1}{2}}) \exp(H_B/RT)}{1+\eta_t \beta_t \delta (a^3/n) N_x (p_o/T^{\frac{1}{2}}) \exp(H_B/RT)} + \frac{\eta_t \alpha_\ell (1-f_b)}{1+\eta_t \beta_t \delta (a^3/n) N_x (p_o/T^{\frac{1}{2}}) \exp(H_B/RT)} \right\} \cdot (p_o/T^{\frac{1}{2}}) \quad (13.a)$$

2) For surface reaction control

$$(da/dt) = \left\{ \frac{\eta_s^2 \beta_s \alpha_b f_b \delta (a^3/n) N_x p_o^{\,m} \exp[(H_B-E_s)/RT]}{1+\beta_s \eta_s \delta (a^3/n) N_x p_o^{\,m} \exp[(H_B-E_s)/RT]} + \frac{\eta_s \alpha_\ell (1-f_b)}{1+\eta_s \beta_s \delta (a^3/n) N_x p_o^{\,m} \exp[(H_B-E_s)/RT]} \right\} \cdot p_o^{\,m} \exp(-E_s/RT) \quad (13.b)$$

3) For diffusion control

$$(da/dt)_{II} = \left\{ \frac{n_d^2 \beta_d \alpha_b f_b \delta (a^3/n) N_x p_o^{\frac{1}{2}} \exp[(2H_B - E_d)/2RT]}{1 + n_d \beta_d \delta (a^3/n) N_x p_o^{\frac{1}{2}} \exp[(2H_B - E_d)/2RT]} \right.$$

$$\left. + \frac{n_d \alpha_\ell (1 - f_b)}{1 + n_d \beta_d \delta (a^3/n) N_x p_o^{\frac{1}{2}} \exp[(2H_B - E_d)/2RT]} \right\} \cdot$$

$$p_o^{\frac{1}{2}} \exp(-E_d/2RT) \qquad (13.c)$$

With the indicated modifications, a new estimate of H_B of 88 kJ/mol is obtained [25]. The difference between this value and the previous estimate of 73 kJ/mol is simply the activation energy for surface reaction (E_s) or 14.7 kJ/mol (rounded to 15 kJ/mol). Using this new value of H_B, it is seen that constant (though different) values of N_{app} are obtained for hydrogen sulfide and for hydrogen (with the exception for the data at 13.3 kPa), Table 3.

This finding is gratifying in that the density of trap site (N_x) is expected to be a material constant and the coefficients β_s, β_t, n_s and n_t are also constants. The difference in N_{app} for hydrogen sulfide and hydrogen reflects differences in the hydrogen supply coefficients (n) and the coefficients for non-equilibrium partitioning (β), and requires further study. The discrepancy between N_{app} for hydrogen at the lowest pressure (13.3 kPa) and those at the other pressures may be attributed to either an underestimation of E_s from the crack growth data or the fact that a transfer to gas-transport control had not been considered.

It should be noted that the modified equations produced no significant improvements in predicting the crack growth response for AISI 4340 steel in hydrogen. Some improvement , however, is obtained in the case of hydrogen sulfide, and is indicated by the dashed curves in Fig. 6.

8. DISCUSSION

The model proposed in this study has successfully combined the achievements obtained from the micromechanism studies [23, 30-32] and the identification of rate controlling processes for hydrogen supply [1,8,9, 28]. This unified "hydrogen partitioning" model successfully predicts the rapid reduction of crack growth rate associated with the change in fracture mode at high temperatures. This model may be of help in gaining insight into the role of microstructural elements on hydrogen embrittlement.

As an example, the effect of prior-austenite grain size on Stage II crack growth rate and crack growth response may be re-examined in terms of this model. In the crack growth rate equations (13.a) to (13.c), a parameter δ is included and represents the volume ratio of grain boundaries to the bulk. If the binding enthalpy H_B, the trap density and the other parameters are assumed to be unaffected by grain size, it can be seen readily that prior-austenite grain size affects only the temperature T_{max}, at which the crack growth rate attains its maximum. As shown in Fig. 7, T_{max} is observed to increase with decreasing grain size. At room temperature, the effect of grain size would not be observed in Stage II crack growth rate data for grain sizes up to 100 μm, because T_{max} would

be equal to or higher than 298K. When the grain size becomes larger than 100 μm, T_{max} drops below 298 K and the coarse grained material may exhibit higher resistance to crack growth, Fig. 7.

The limiting case is that of a single crystal where the volume ratio δ becomes zero. The crack growth rate is expected to be much slower because of the absence of grain boundaries. The mean crack growth rate $(da/dt)_{II}$ can then be described simply by Eqn. (14).

$$(da/dt)_{II} = \alpha_{\ell}\dot{Q} \tag{14}$$

It should be noted that, however, the contribution of quasi-cleavage was neglected in deriving the crack growth equations. In the absence of grain boundaries, quasi-cleavage may play an important role in hydrogen embrittlement. Exclusion of its contribution, therefore, may not be reasonable for single crystals and for coarse grained materials.

The contribution of quasi-cleavage to hydrogen embrittlement can be readily estimated from the consideration of hydrogen-dislocation interactions. The crack growth rate can then be described as follows:

$$(da/dt)_{II} = (\alpha_q f_q \kappa_q + \alpha_{\ell} f_{\ell} \kappa_{\ell})\dot{Q} \tag{15}$$

In Eqn. (15), κ_q and κ_{ℓ} are the hydrogen distribution coefficients for quasi-cleavage and for lattice; respectively, and are given as follows:

$$\kappa_q = \frac{\delta' C_q/C_{\ell}}{1+\delta' C_q/C_{\ell}} \text{ and } \kappa_{\ell} = \frac{1}{1+\delta' C_q/C_{\ell}} \tag{16.a}$$

$$C_q/C_{\ell} = \tau(a^3/n)N_{xq} \exp(H_q/RT) \tag{16.b}$$

where N_{xq} is the trapping density for quasi-cleavage, δ' is the volume fraction of quasi-cleavage sites, H_q is the binding enthalpy for hydrogen to the quasi-cleavage planes.

The proposed model can be readily extended to an examination of the hydrogen-AISI 4130 steel system studied by Williams et al. [1-3]*. Without changing the binding enthalpy H_B, good agreement is obtained between the present model and their experimental data. The comparison is shown in Fig. 8, where $f_b = 1$ and $f_\ell = 0$ are assumed. It should be noted that the form of crack growth rate equation given by the present model (Eqns. 16.a to 16.c) and that given by Williams and Nelson [1-3] are nearly the same. This similarity in form, however, does not indicate agreement, because the physical bases of these two models are very different. The Williams and Nelson model attributed the reduction of crack growth rate at the high temperatures to the reduction in hydrogen supply rate. The present model, on the other hand, attributes this change to a partitioning of hydrogen amongst the different microstructural sites with changes in temperature.

The effect of adsorption equilibrium, however, must still be considered as an additional contribution to the present model. For surface reaction controlled process, substituting the hydrogen supply rate, $\dot{Q}$, given by Williams and Nelson into the present model, one can readily show that the crack growth equation at high temperatures reduces to the following form [25].

*Note that the Williams and Nelson data were obtained for a fixed K_I, and do not necessarily correspond to Stage II crack growth over the entire temperature range.

$$\ell n(da/dt)_{II} = \ell n\ C + \left(\frac{H_B+2\Delta H-2E_s}{RT}\right) \qquad (17)$$

The quantity C is approximately constant if the weak temperature dependence of f_b and $T^{-\frac{1}{2}}$ is neglected.

Let the binding enthalpy to the grain boundaries, (H_B), be equal or greater than 58.6 kJ/mol and the apparent activation energy for surface reaction E_s = 14.7 kJ/mol, then the heat of absorption, ΔH, needs to be equal to or less than 14.7 kJ/mol to conform to the high-temperature crack growth data. This preliminary result clearly shows that the apparent heat of adsorption (ΔH) is relatively small in comparison with the binding enthalpy to the grain boundaries. As such, the contribution of adsorption equilibrium to the change in crack growth response in Region C is rather small.

The proposed model can also account for the change in Stage II crack growth rate from Region A to Region C in the 18Ni maraging steels. It cannot, however, explain the sudden drop off in crack growth rates at the higher temperatures, see Fig. 9. Mechanisms involving two-dimensional grain boundary surface phase transformation, suggested by Gangloff and Wei [4,5] and Chan, Klier, and Wei [34], could provide a good fit to the experimental p-T conditions for the sudden drop off in Stage II crack growth rate. The features of the interaction of hydrogen with particular components of the steels that account for the specific responses, however, are still unclear. Further determination of the relationship between grain boundary composition and conditions of phase equilibria involving hydrogen is essential to the development of high strength steels with high resistance to hydrogen assisted crack growth [34].

9. SUMMARY

Results of the current study have provided an accurate characterization of the crack growth response for high strength steel exposed to gaseous H_2 and H_2S. The principal results from this study are summarized as follows:

1. A model which combines recent achievements from studies of micromechanisms of cracking and of rate controlling processes for environmentally assisted crack growth is proposed.

2. The model suggests that the main crack growth response for hydrogen-assisted cracking is essentially determined by two basic factors: (a) the rate of hydrogen supplied to the fracture process zone, which is controlled by one of the rate controlling processes previously identified, and (b) the partitioning of hydrogen amongst the different microstructural elements or traps (principally between prior-austenite grain boundaries and the matrix), which is controlled by the hydrogen-trap interactions and determines the micro-crack growth rate for each element. The different micromechanisms are assumed to operate in parallel.

3. Quantitative evaluation of the model in relation to crack growth response has been carried out. By including experimentally observed changes in fracture morphology, very good agreement between the model predictions and observed crack growth responses for AISI 4340 and 4130 steels in H_2 and H_2S is obtained.

4. Partitioning of hydrogen between prior-austenite grain boundaries and matrix is shown to be a more reasonable explanation for the observed crack growth response at "high" temperature, versus the explanations offered by the surface reaction models.

5. Crack growth response is consistent with a binding enthalpy of hydrogen to the prior-austenite grain boundaries of about 90 kJ/mol (vs. about 60 kJ/mol reported by Hirth for iron).

6. The contribution of prior-austenite grain size to hydrogen embrittlement was examined by the model. The room temperature crack growth rate is not expected to be sensitive to grain size up to 100 μm. For grain size larger than 100 μm, the room temperature crack growth rate may decrease with increasing grain size. The fact that single crystals have the highest resistance to hydrogen cracking is consistent with the model.

7. Adsorption equilibrium proposed by Williams et al. was considered in relation to the proposed model for surface reaction controlled crack growth. Preliminary estimates indicated that the apparent heat of adsorption may be relatively small and is less than 15 kJ/mol. As such, the contribution of adsorption equilibrium is not expected to be an important cause for the decrease in crack growth rates at "high" temperatures.

8. Neither partitioning of hydrogen nor adsorption equilibrium can account for the observed "high" temperature response of 18Ni maraging steel in hydrogen. The two-dimensional phase transformation model proposed by Chan, Klier and Wei is currently the only reasonable alternative and requires further study.

ACKNOWLEDGEMENT

This research was supported in part by the Office of Naval Research under Contracts N00014-75-C-0543 and N00014-83-K-0107, NR036-097.

Appendix I: Equilibrium Partition of Hydrogen

Following Hirth [23], the appropriate reaction for hydrogen with a single trap site X is given by Eqn. (I-1)

$$\underline{H} + X \rightleftharpoons HX \tag{I-1}$$

The corresponding equilibrium partitioning of hydrogen can be expressed by either the Boltzmann [22] or the Fermi-Dirac Statistics [23]:

$$H_X = H_\ell \exp(H_B/RT) \tag{I-1a}$$

$$H_X/(1-Hx) \simeq H_\ell \exp(H_B/RT) \tag{I-1b}$$

where H_X and H_ℓ are the concentrations of hydrogen about the trap sites and in the lattice (in atom fraction) respectively.

In considering the partitioning of hydrogen between grain boundaries and the lattice, the following relationships between atom fraction and molal concentration is used:

$$C_{Hx} = (N_X/2N_A)H_X \tag{I-2a}$$

$$C_\ell = (N_O/2N_A)H_\ell \simeq [(n/a^3)/2N_A]H_O \tag{I-2b}$$

In Eqns. (I-2a) and (I-2b), N_X is the density of trap sites in the grain boundaries (numbers/m^3); N_O is the density of perfect lattice sites and can be approximated by n/a^3, where a is the lattice parameter of the metal and n is the number of atoms per unit cell; and N_A is the Avogadro's constant. The corresponding equilibrium partitioning of hydrogen between the grain boundary trap sites and the lattice (in molal concentrations) can be expressed as follows:

$$C_{Hx} = C_{\ell}(a^3/n)N_x \exp(H_B/RT) \qquad \text{Boltzmann} \qquad \text{(I-3a)}$$

$$C_{Hx} = \frac{(a^3/n)N_x C_{\ell} \exp(H_B/RT)}{1+2(a^3/n)N_A C_{\ell} \exp(H_B/RT)} \qquad \text{Fermi-Dirac} \qquad \text{(I-3b)}$$

Appendix II: Estimation of Parameters from Crack Growth Data

The crack growth rate and hydrogen partition equations contain a number of parameters that must be prescribed or estimated from the experimental data. For the lattice parameter (a), a value of 0.287 nm for α-iron is used. The number of atoms per unit cell n is equal to 2. The volume ratio between the prior-austenite grain boundaries and the bulk, δ, is estimated to be 10^{-4}, based on an average prior-austenite grain size of 20 μm for the steel used in this study and an assumed grain boundary thickness of 1 nm. The other coefficients, namely η's, α's (or the product $\eta\alpha$) and H_B, are estimated by matching the crack growth rate equations to the experimental data over specific temperature regions. The detailed estimation procedures are given in the following subsections.

Estimation of $\eta_t\alpha_b$, $\eta_s\alpha_b$ and $\eta_d\alpha_b$.

By examining Eqns. (8a), (10) and (11), it can be seen that the term $C_b/C_\ell = (a^3/n)N_x \exp(H_B/RT)$ is much greater than one in the low temperature region. Hence the prior-austenite grain boundaries are essentially saturated with hydrogen (κ_b=1), and cracking is expected to occur principally along these boundaries, with f_b=1. The crack growth relations, Eqn. (10), then reduces to the following form:

$$(da/dt)_{II} = \begin{cases} \eta_t\alpha_b(p/T^{1/2}) & \text{Transport} \quad \text{(II-1a)} \\ \eta_s\alpha_b p^m \exp(-E_s/RT) & \text{Surface Reaction} \quad \text{(II-1b)} \\ \eta_d\alpha_b p^{1/2}\exp(-E_d/2RT) & \text{Diffusion} \quad \text{(II-1c)} \end{cases}$$

These equations are identical in form to those given by Wei [11]. Equation (II-1) can be used to determine the coefficients $\eta_t\alpha_b$, $\eta_s\alpha_b$ and $\eta_d\alpha_b$ from the experimental data on crack growth [25].

Estimation of $\eta_t\alpha_\ell$, $\eta_s\alpha_\ell$ and $\eta_d\alpha_\ell$

In the high temperature region, the term C_b/C_ℓ becomes very small, and κ_ℓ then approaches one. In other words, most of the hydrogen now goes into the matrix and cracking is expected to occur fully by micro-void coalescence (i.e., f_ℓ=1). In this case, $(da/dt)_{II}$ reduces to the following form:

$$(da/dt)_{II} = \begin{cases} \eta_t\alpha_\ell(p/T^{\frac{1}{2}}) & \text{Transport} \quad \text{(II-2a)} \\ \eta_s\alpha_\ell p^m \exp(-E_s/RT) & \text{Surface Reaction} \quad \text{(II-2b)} \\ \eta_d\alpha_\ell p^{\frac{1}{2}} \exp(-E_d/2RT) & \text{Diffusion} \quad \text{(II-2c)} \end{cases}$$

Equation (II-2) may be used to estimate the coefficients $\eta_t\alpha_\ell$, $\eta_s\alpha_\ell$ and $\eta_d\alpha_\ell$ from the appropriate crack growth data [25].

Estimation of Binding Enthalpy, H_B

It is recognized that, at the early stage of transition into Region C with increases in test temperature, the areal fraction of intergranular (i.e. grain boundary) separation is almost equal to 1 [16,25]. Also, the rate of crack growth by micro-void coalescence is negligibly small in comparison with that by grain boundary separation (i.e., α_ℓ is at least 3 orders of magnitude below α_b [25]). The contribution of micro-void

coalescence to the crack growth rate $(da/dt)_{II}$, therefore, may be ignored. Equation (10) then can be reduced to the following form:

$$(da/dt)_{II} = \begin{cases} \eta_t \alpha_b f_b \tau \delta (a^3/n) N_x (p/T^{1/2}) \exp(H_B/RT) & \text{(II-3a)} \\ \eta_s \alpha_b f_b \tau \delta (a^3/n) N_x p^m \exp[(H_B - E_s)/RT] & \text{(II-3b)} \\ \eta_d \alpha_b f_b \tau \delta (a^3/n) N_x p^{1/2} \exp[(2H_B - E_d)/2RT] & \text{(II-3c)} \end{cases}$$

Equation (II-3) can be used to estimate the binding enthalpy for hydrogen to the prior-austenite grain boundaries (H_B) from the experimental data on Stage II crack growth in the lower temperature portion of Region C.

For this estimate, Eqn. (II-3b) and the data for surface reaction controlled growth in an AISI 4340 steel at a hydrogen pressure of 133 kPa [7] are used. In Eqn. (II-3b), all the coefficients except f_b and τ are constant for a given material and environment. Fractographic analyses have shown that f_b varied from 1 to 0.8 when the temperature was increased from region A up to the highest temperature tested in Region C [16,25]. Because of this weak dependence on temperature, $f_b \simeq 1$ is assumed. The non-equilibrium coefficient, τ, may be assumed to depend either strongly or weakly on temperature. In either case, τ can be considered as a constant for a given pressure (see sections 6 and 7). Finally, from a plot of $\ell n(da/dt)$ vs. $1/T$ shown in Fig. (II-1)[7], the binding enthalpy of hydrogen to the prior-austenite grain boundaries is estimated to be approximately 73 kJ/mol. This value is higher than, but is still comparable to, the value of 58.6 kJ/mol suggested by Hirth [23].

REFERENCES

1. D. P. Williams and H. G. Nelson: Met. Trans. A, 1970, vol. 1A, p. 63.

2. H. G. Nelson, D. P. Williams and A. S. Tetelman: Met. Trans. A, 1971, vol. 2A, p. 953.

3. H. G. Nelson and D. P. Williams: in Stress Corrosion Cracking and Hydrogen Embrittlement of Iron Base Alloys, R. W. Staehle, J. Hochmann, R. D. McCright and J. E. Slater, eds., NACE-5, Houston, Texas, 1978, p. 390.

4. R. P. Gangloff and R. P. Wei: Met. Trans. A, 1977, vol. 8A, p. 1043.

5. R. P. Gangloff and R. P. Wei: ASTM STP 645, American Society for Testing and Materials, Philadelphia, PA, 1978, p. 87.

6. G. W. Simmons, P. S. Pao and R. P. Wei: Met. Trans., 1978, vol. 9A, p. 1147.

7. M. C. Lu, P. S. Pao, N.H. Chan, K. Klier and R. P. Wei: in Proceedings of Second Japan Institute of Metals International Symposium (JIMIS-2), Hydrogen in Metals, Suppl to Trans. Japan Inst. Metals, 1980, vol. 21, p. 449.

8. N. H. Chan, K. Klier and R. P. Wei: in Proceedings of Second Japan Institute of Metals International Symposium (JIMIS-2), Hydrogen in Metals, Suppl. to Trans. Japan Inst. Metals, 1980, vol. 21, p. 305.

9. M. C. Lu, P. S. Pao, T. W. Weir, G. W. Simmons and R. P. Wei: Met. Trans. A, 1980, vol. 12A, p. 805.

10. R. P. Wei, K. Klier, G. W. Simmons and Y. T. Chou: in Hydrogen Embrittlement and Stress Corrosion Cracking, American Society for Metals, Metals Park, OH, 1984, p. 103 (in press).

11. R. P. Wei: in Hydrogen Effects in Metals, I. M. Bernstein and A. W. Thompson, eds., TMS-AIME, Warrendale, PA, 1981, p. 677.

12. H. G. Nelson: NASA TN D-6691, National Aeronautic and Space Administration, 1972.

13. R. W. Pasco and P. J. Ficalora: Scripta Met., 1980, vol. 15, p. 1019.

14. R. W. Pasco, K. Sieradzki and P. J. Ficalora: Scripta Met., 1982, vol. 16, p. 881.

15. J. A. Schwarz and H. W. Liu: Scripta Met., 1980, vol. 15, p. 839.

16. Ming Gao, M. Lu and R. P. Wei: Met. Trans. A, 1984, vol. 15A, p. 735.

17. Ming Gao: M.S. Thesis, Lehigh University, Bethlehem, PA, 1982.

18. A. J. Stavros and H. W. Paxton: Met. Trans. A, 1970, vol. 1A, p. 3049.

19. G. Lapasset, J. P. Laurent, M. Aucouturier and P. Lacombe: in l'Hydrogen dans les Mètaux Congrès International, Editions Science et Indusie, Paris, 1972, p. 108.

20. A. Vassel, G. Lapasset, J. P. Laurent, M. Aucouturier and P. Lacombe: ibid., p. 348.

21. T. Asaoka, G. Lapasset, M. Aucouturier and P. Lacomba: Corrosion, 1978, vol. 34, p. 39.

22. A. H. Cottrell: in Dislocation and Plastic Flow in Crystals, Oxford Press, Amen House, London, 1965.

23. J. P. Hirth: Met. Trans. A, 1980, vol. 11A, p. 861.

24. J. O'M. Bockris: in Stress Corrosion Cracking and Hydrogen Embrittlement of Iron Base Alloys, R. W. Staehle, J. Hochmann, R. D. McCright, and J. E. Slater, eds., NACE-5, Houston, Texas, 1978, p. 286.

25. Ming Gao: Ph.D. Thesis, Lehigh University, Bethlehem, PA, 1983.

26. T. W. Weir, G. W. Simmons, R. G. Hart and R. P. Wei: Scripta Met., 1980, vol. 14, p. 357.

27. S. Glasstone, K. J. Laidler, and H. Eyring: in The Theory of Rate Processes, McGraw Hill, 1948, p. 339.

28. M. C. Lu, Y. T. Chou and R. P. Wei: "A Model for Diffusion Controlled Crack Growth in Gaseous Environment", unpublished results, Lehigh University, 1980.

29. G. M. Pressouyre and I. M. Bernstein: Met. Trans. A, 1978, vol. 9A, p. 1571.

30. R. Gibala and D. S. DeMegli: in Hydrogen Effects in Metals, I. M. Bernstein and A. W. Thompson, eds., ASM, Metals Park, OH, 1981, p. 113.

31. R. Gibala: in Stress Corrosion Cracking and Hydrogen Embrittlement of Iron Base Alloys, R. W. Staehle, J. Hochmann, R. D. McCright, and J. E. Slater, eds., NACE-5, Houston, Texas, 1978, p. 244.

32. A. P. Miodownik: ibid., p. 272.

33. P. S. Pao and R. P. Wei: Scripta Met., 1977, vol. 11, p. 515.

34. N. H. Chan, K. Klier and R. P. Wei: Scripta Met., 1978, vol. 12, p. 1043.

Table 1: Parameters Associated with Modeling of Crack Growth for AISI 4340 Steel in Hydrogen.

Hydrogen Pressure	$\eta_s \alpha_b$	$\eta_s \alpha_\ell$	E_s	H_B	a	δ	N_{app} (τN_x)
kPa	$(m/s)(kPa)^{1/2}$	$(m/s)(kPa)^{1/2}$	kJ/mol	kJ/mol	nm	μm	m^{-3}
133	2.8×10^{-3}	1×10^{-6}	14.7	73	0.287	10^{-4}	3.8×10^{22}
57	2.1×10^{-3}	1×10^{-6}	14.2	73	0.287	10^{-4}	2.8×10^{22}
13.3	1.2×10^{-3}	1×10^{-6}	8.8	73	0.287	10^{-4}	8.5×10^{21}

Table 2: Parameters Associated with Modeling of Crack Growth for AISI 4340 Steel in Hydrogen Sulfide.

Hydrogen Sulfide Pressure	$\eta_t \alpha_b$	$\eta_t \alpha_\ell$	E_s	H_B	a	δ	N_{app} (τN_x)
kPa	$(m/s)K^{1/2}(kPa)$	$(m/s)K^{1/2}(kPa)$	kJ/mol	kJ/mol	nm	μm	m^{-3}
2.66	2.8×10^{-3}	1×10^{-6}	NA	73	0.287	10^{-4}	4.2×10^{23}
0.133	2.1×10^{-3}	1×10^{-6}	NA	73	0.287	10^{-4}	3.6×10^{22}

Table 3: Parameters Associated with the Modified Model for Crack Growth in AISI 4340 Steel.

a. Hydrogen

Pressure kPa	E_s kJ/mol	H_B kJ/mol	$N_{app} \propto \beta_s \eta_s N_x$ $(kPa)^{-1} m^{-3}$
133	14.7	88	3.42×10^{21}
57	14.2	88	3.42×10^{21}
13.3	8.8	88	2.99×10^{20}

b. Hydrogen Sulfide.

Pressure kPa	E_s kJ/mol	H_B kJ/mol	$N_{app} \propto \beta_t \eta_t N_x$ $K(kPa)^{-1} m^{-3}$
2.66		88	5.39×10^{21}
0.133		88	5.39×10^{21}

Note: δ, $\eta_s \alpha_b$, $\eta_s \alpha_\ell$, $\eta_t \alpha_b$ and $\eta_t \alpha_\ell$ are given in Tables 1 and 2.

LIST OF FIGURES

Fig. 1: Schematic illustration of sequential processes involved in the embrittlement of ferrous alloys by external environments. (Embrittlement reaction is depicted schematically by the Fe-H-Fe bond.) [4,11]

Fig. 2: The temperature dependence and the corresponding rate controlling processes for Stage II crack growth in various hydrogenous environments: (a) H_2S at 2.66 kPa, (b) H_2S at 0.133 kPa, (c) H_2 at 133 kPa and (d) H_2O (liquid) [11].

Fig. 3: Illustration of subdivision of hydrogen assisted cracking sequence into supply, partitioning and embrittlement portions [16].

Fig. 4: Schematic illustration of hydrogen concentration in the crack tip region for a crack moving at a constant (Stage II) rate.

Fig. 5: Comparison between model predictions and data for AISI 4340 steel tested in hydrogen at three pressures [7,16].

Fig. 6: Comparison between model predictions and data for AISI 4340 steel tested in hydrogen sulfide at two pressures [9].

Fig. 7: Predicted effect of prior-austenite grain size on Stage II crack growth rate in hydrogen.

Fig. 8: Comparison between model predictions and data for AISI 4130 steel tested in hydrogen at two strength levels [3].

Fig. 9: Comparison between model predictions and data for three maraging steels tested in hydrogen at 133 kPa [33].

Fig. II-1: The temperature dependence for Stage II crack growth in high temperature region (Region C) at 133 kPa of hydrogen pressure.

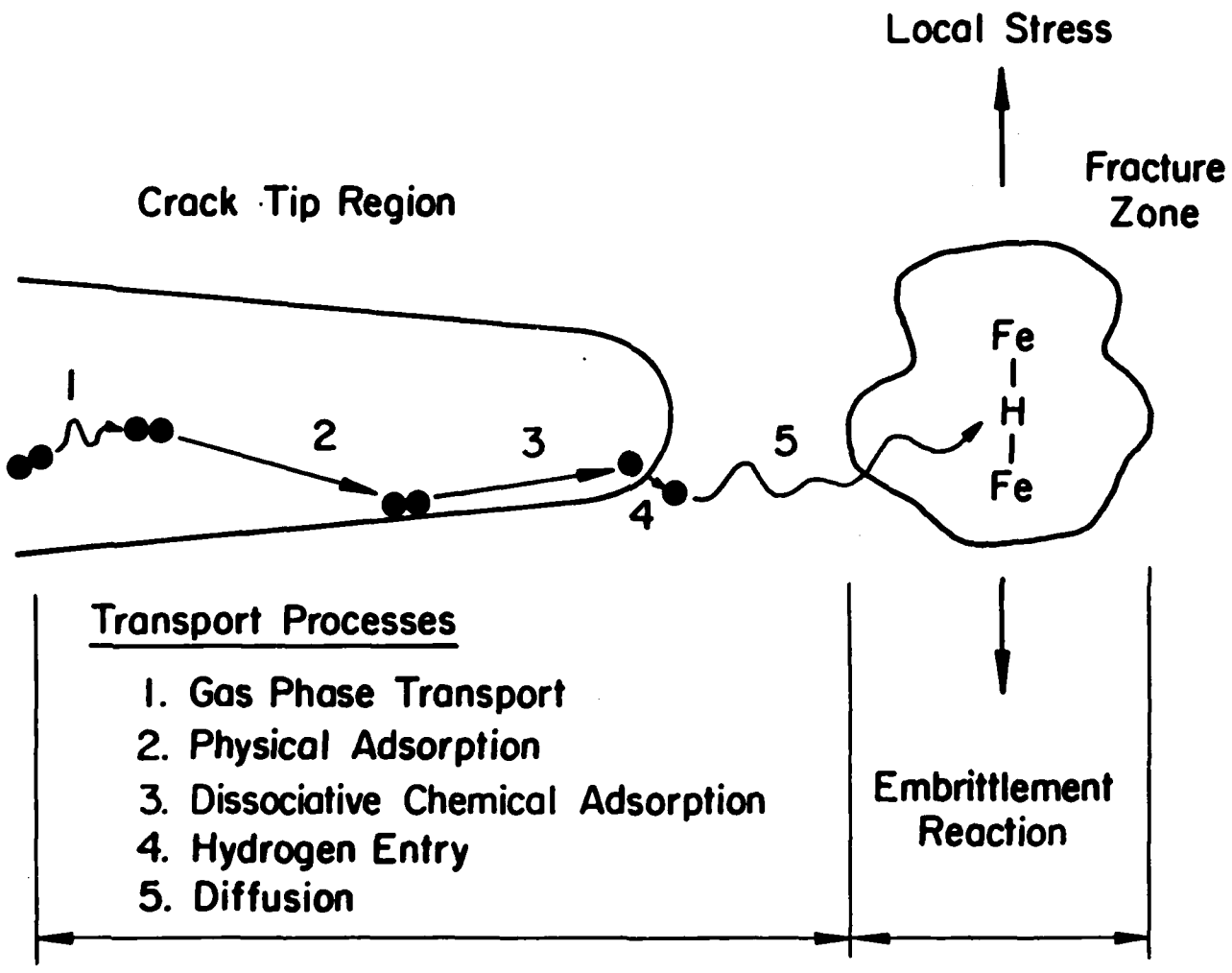

Fig. 1: Schematic illustration of sequential processes involved in the embrittlement of ferrous alloys by external environments. (Embrittlement reaction is depicted schematically by the Fe-H-Fe bond.) [4,11]

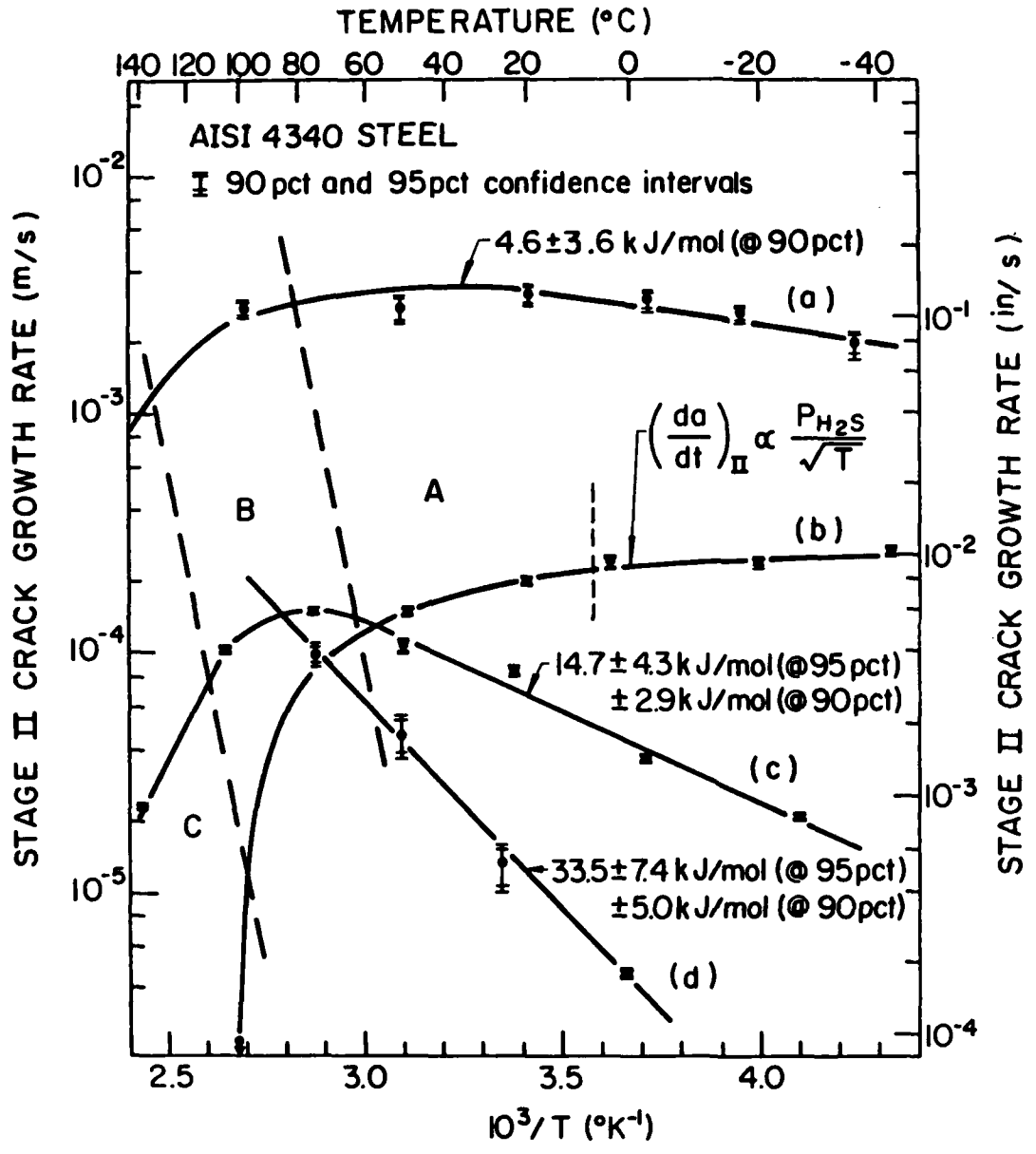

RATE CONTROLLING PROCESS

(a) Diffusion

(b) Gas Phase Transport

(c) Surface Reaction (H_2 - Metal)

(d) Surface Reaction (H_2O - Metal)

Fig. 2: The temperature dependence and the corresponding rate controlling processes for Stage II crack growth in various hydrogenous environments: (a) H_2S at 2.66 kPa, (b) H_2S at 0.133 kPa, (c) H_2 at 133 kPa, and (d) H_2O (liquid) [11].

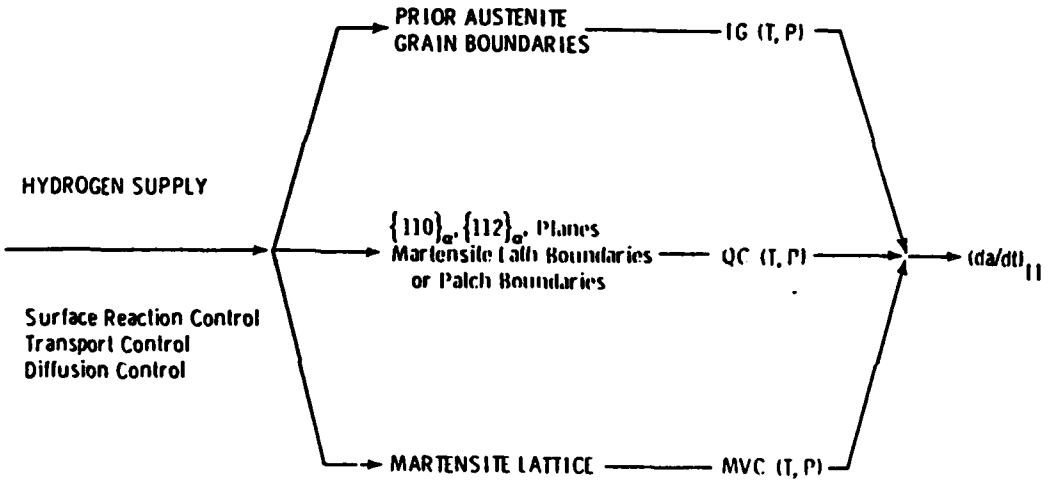

Fig. 3: Illustration of subdivision of hydrogen assisted cracking sequence into supply, partitioning and embrittlement portions [16].

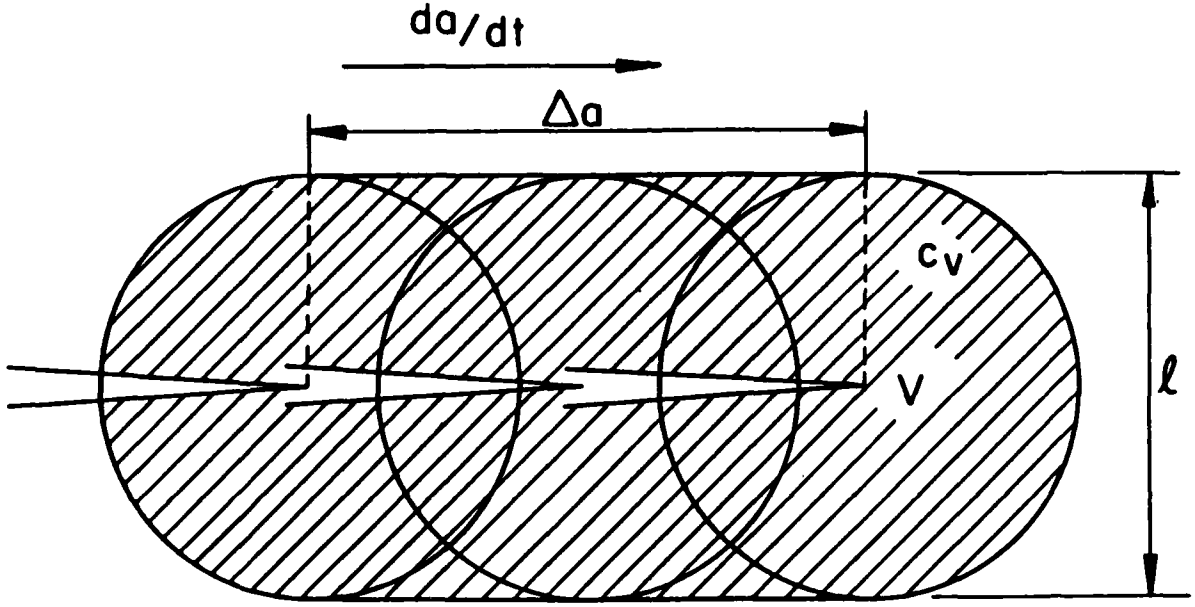

V = Fracture Process Zone

c_V = Hydrogen Concentration in Fracture Process Zone

Fig. 4: Schematic illustration of hydrogen concentration in the crack tip region for a crack moving at a constant (Stage II) rate.

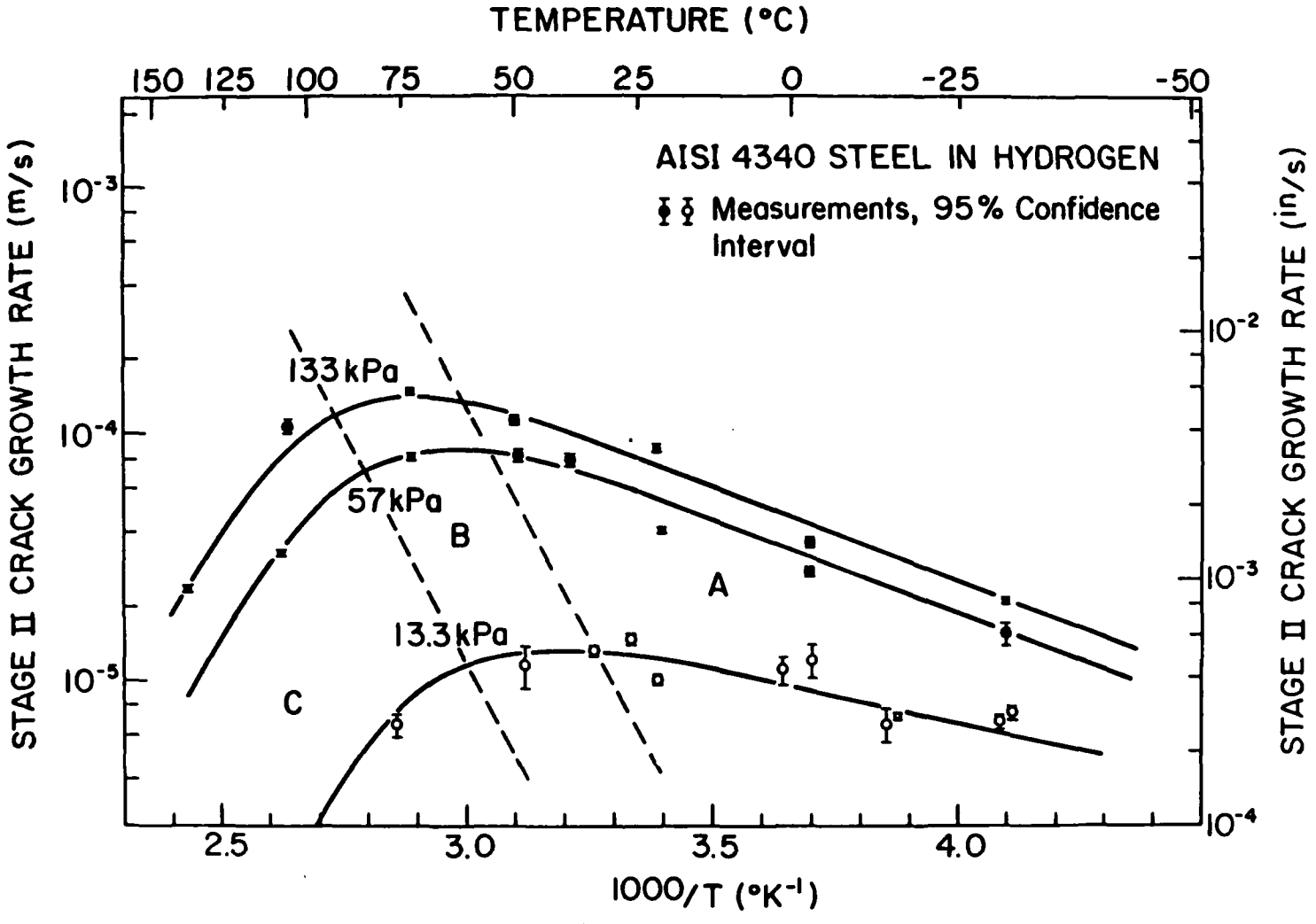

Fig. 5: Comparison between model predictions and data for AISI 4340 steel tested in hydrogen at three pressures [7,16].

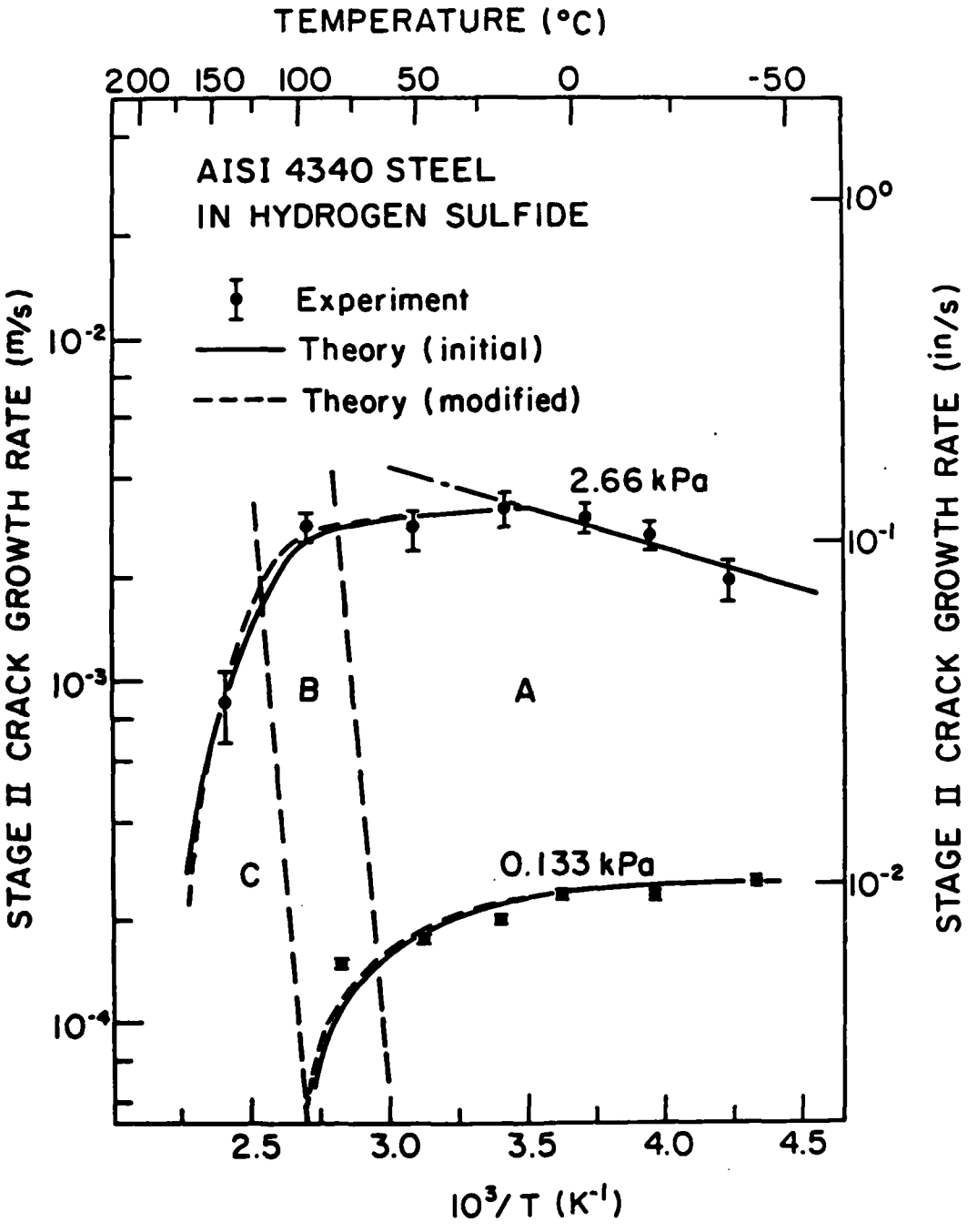

Fig. 6: Comparison between model predictions and data for AISI 4340 steel tested in hydrogen sulfice at two pressures [9].

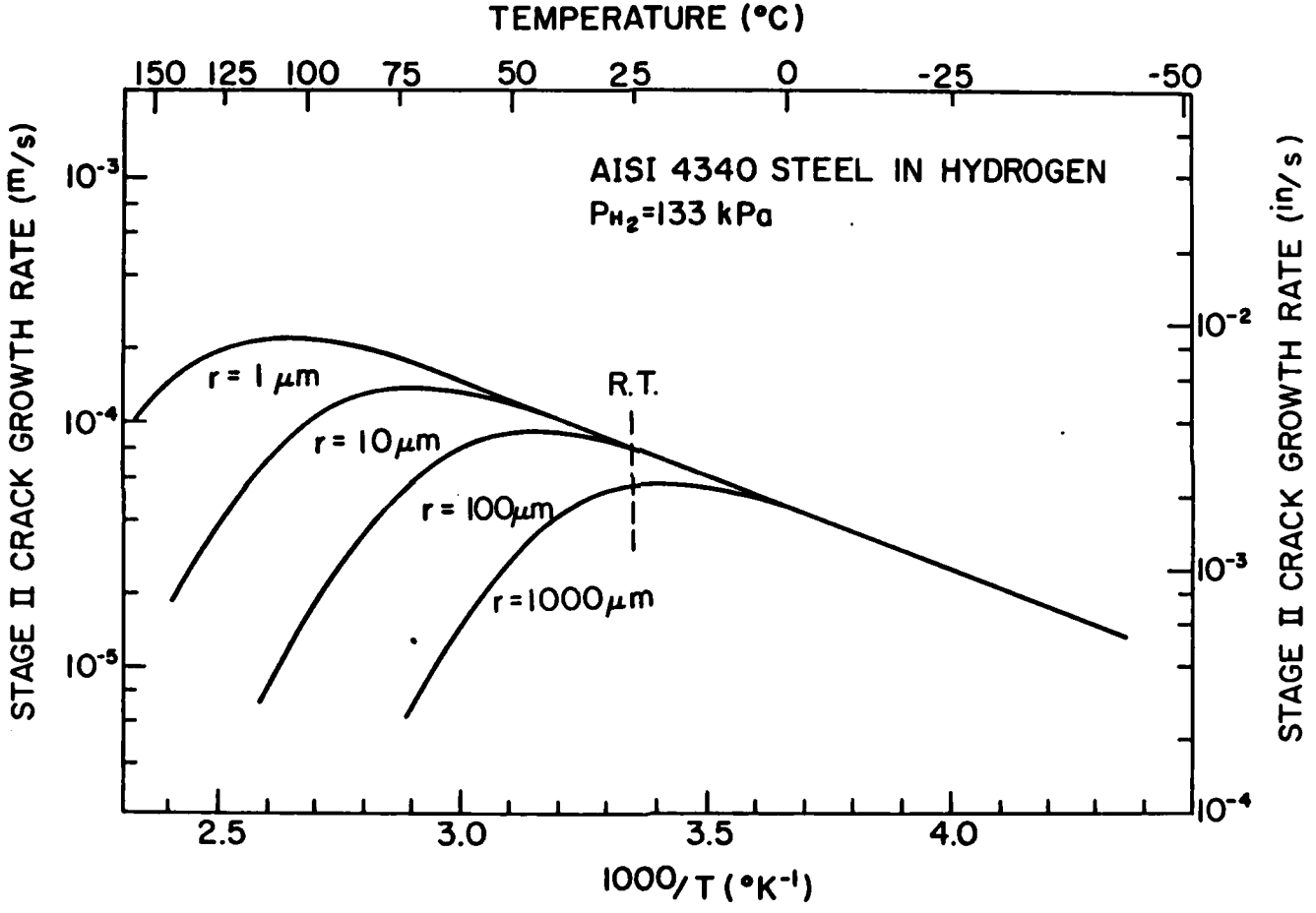

Fig. 7: Predicted effect of prior-austenite grain size on Stage II crack growth rate in hydrogen.

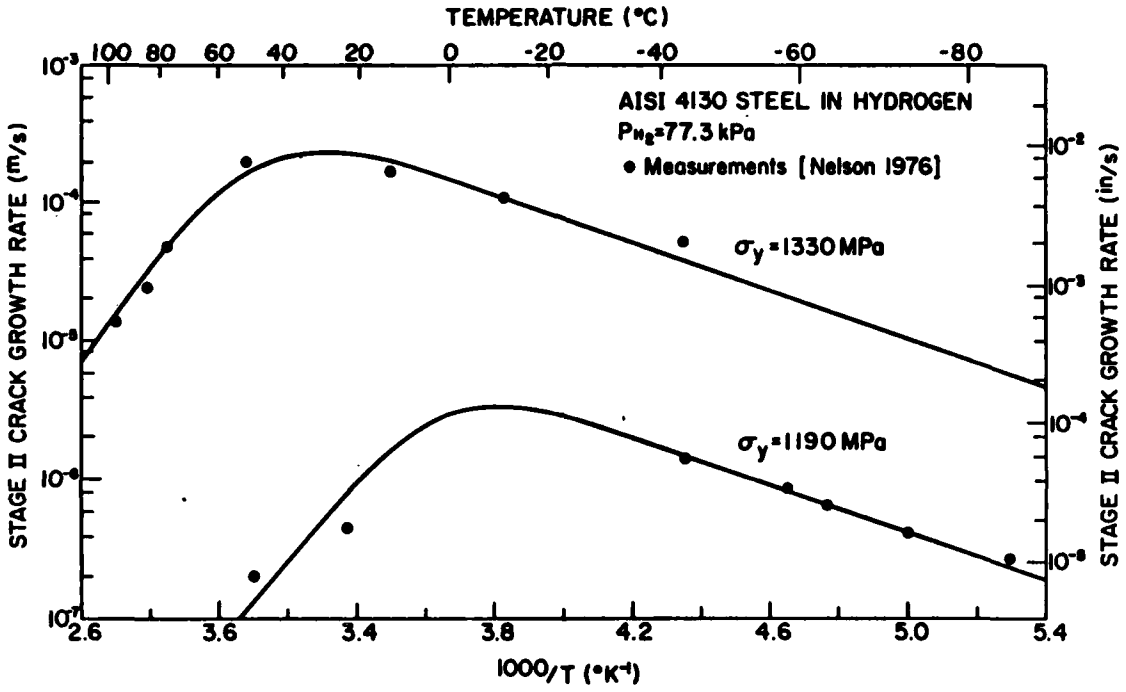

Fig. 8: Comparison between model predictions and data for AISI 4130 steel tested in hydrogen at two strength levels [3].

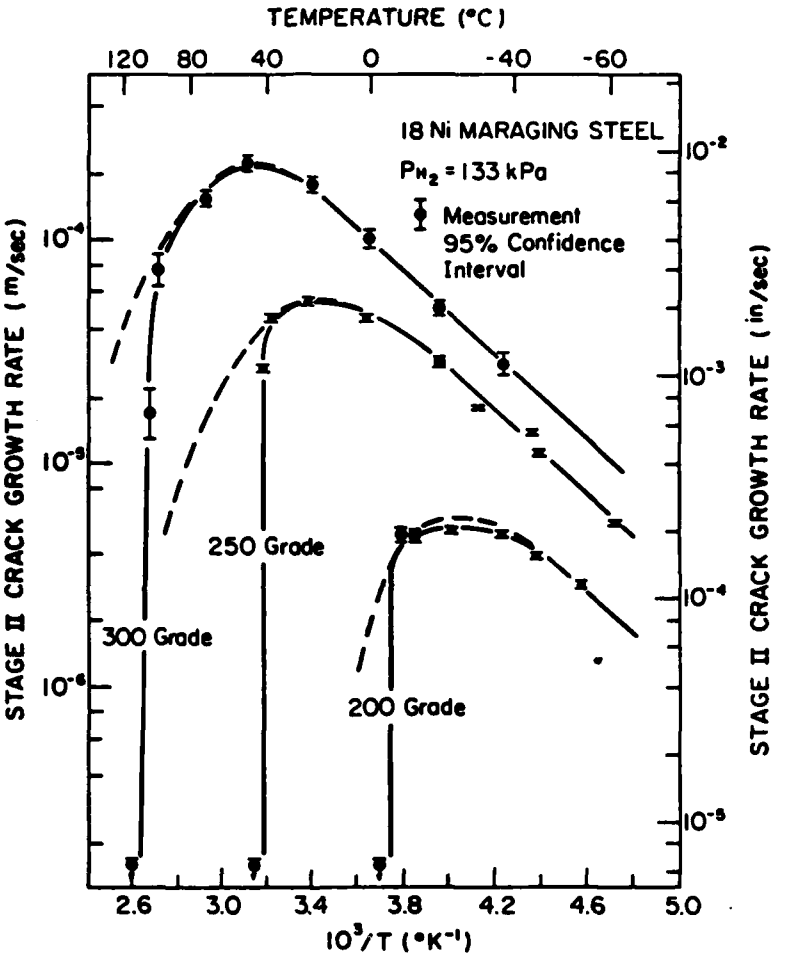

Fig. 9: Comparison between model predictions and data for three maraging steels tested in hydrogen at 133 kPa [33].

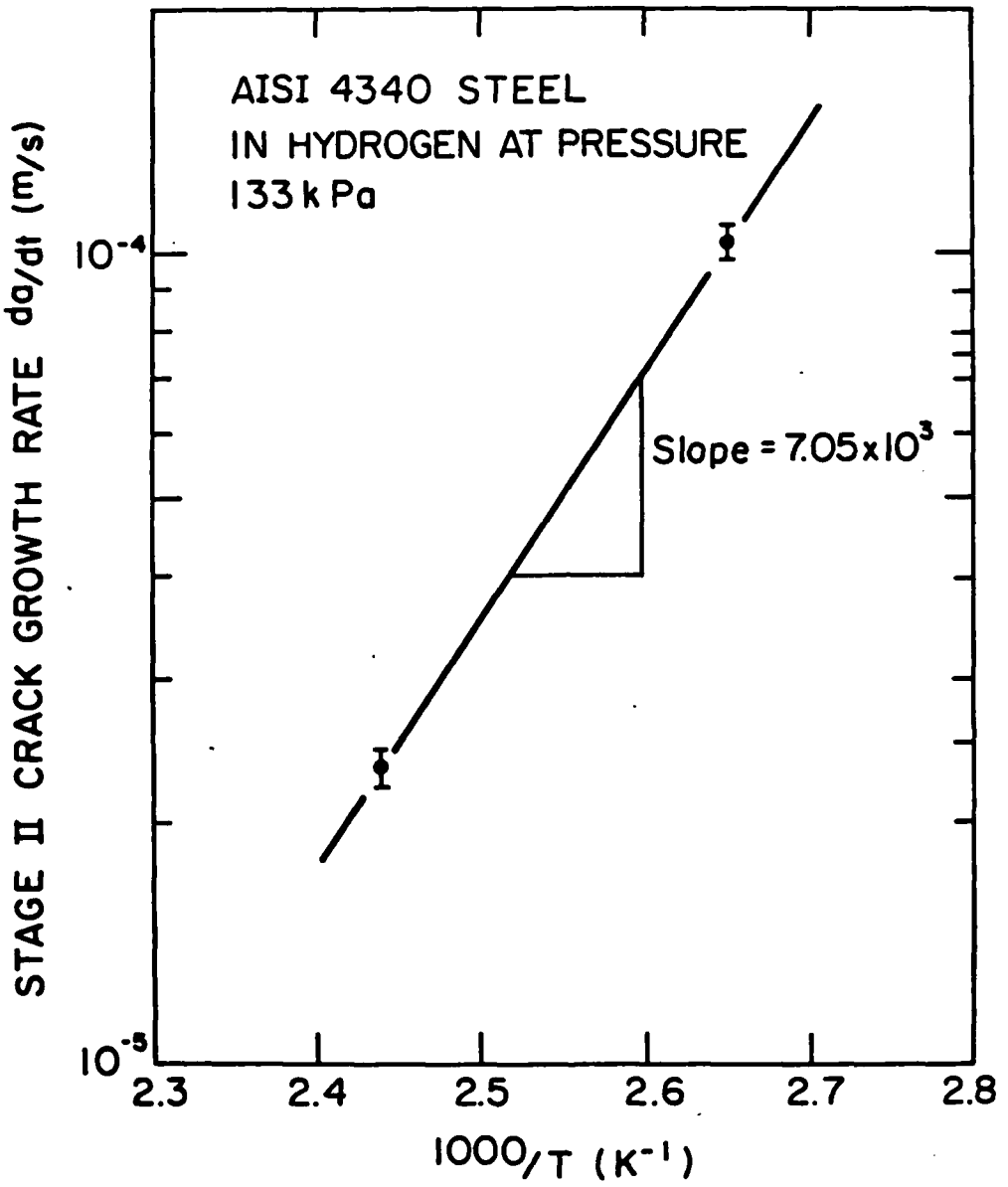

Fig. II-1: The temperature dependence for Stage II crack growth in high temperature region (Region C) at 133 kPa of hydrogen pressure.

BASIC DISTRIBUTION LIST

Technical and Summary Reports April 1978

Organization	Copies
Defense Documentation Center Cameron Station Alexandria, VA 22314	12
Office of Naval Research Department of the Navy 800 N. Quincy Street Arlington, VA 22217	
ATTN: Code 471	1
Code 102	1
Code 470	1
Commanding Officer Office of Naval Research Branch Office Building 114, Section D 666 Summer Street Boston, MA 02210	1
Commanding Officer Office of Naval Research Branch Office 536 South Clark Street Chicago, IL 60605	1
Office of Naval Research San Francisco Area Office One Hallidie Plaza Suite 601 San Francisco, CA 94102	1
Naval Research Laboratory Washington, DC 20375	
ATTN: Codes 6000	1
6100	1
6300	1
6400	1
2627	1
Naval Air Development Center Code 302 Warminster, PA 18964 ATTN: Mr. F. S. Williams	1

Organization	Copies
Naval Air Propulsion Test Center Trenton, NJ 08628 ATTN: Library	1
Naval Construction Batallion Civil Engineering Laboratory Port Hueneme, CA 93043 ATTN: Materials Division	1
Naval Electronics Laboratory San Diego, CA 92152 ATTN: Electron Materials Sciences Division	1
Naval Missile Center Materials Consultant Code 3312-1 Point Mugu, CA 92041	1
Commanding Officer Naval Surface Weapons Center White Oak Laboratory Silver Spring, MD 20910 ATTN: Library	1
David W. Taylor Naval Ship Research and Development Center Materials Department Annapolis, MD 21402	1
Naval Undersea Center San Diego, CA 92132 ATTN: Library	1
Naval Underwater System Center Newport, RI 02840 ATTN: Library	1
Naval Weapons Center China Lake, CA 93555 ATTN: Library	1
Naval Postgraduate School Monterey, CA 93940 ATTN: Mechanical Engineering Department	1

BASIC DISTRIBUTION LIST (cont'd)

Organization	Copies
Naval Air Systems Command Washington, DC 20360 ATTN: Codes 52031 52032	1
Naval Sea System Command Washington, DC 20362 ATTN: Code 035	1
Naval Facilities Engineering Command Alexandria, VA 22331 ATTN: Code 03	1
Scientific Advisor Commandant of the Marine Corps Washington, DC 20380 ATTN: Code AX	1
Naval Ship Engineering Center Department of the Navy Washington, DC 20360 ATTN: Code 6101	1
Army Research Office P.O. Box 12211 Triangle Park, NC 27709 ATTN: Metallurgy & Ceramics Program	1
Army Materials and Mechanics Research Center Watertown, MA 02172 ATTN: Research Programs Office	1
Air Force Office of Scientific Research Bldg. 410 Bolling Air Force Base Washington, DC 20332 ATTN: Chemical Science Directorate Electronics & Solid State Sciences Directorate	1 1
Air Force Materials Laboratory Wright-Patterson AFB Dayton, OH 45433	1
Library Building 50, Rm 134 Lawrence Radiation Laboratory Berkeley, CA	1

Organization	Copies
NASA Headquarters Washington, DC 20546 ATTN: Code RRM	1
NASA Lewis Research Center 21000 Brookpark Road Cleveland, OH 44135 ATTN: Library	1
National Bureau of Standards Washington, DC 20234 ATTN: Metallurgy Division Inorganic Materials Div.	1 1
Director Applied Physics Laboratory University of Washington 1013 Northeast Forthieth Street Seattle, WA 98105	1
Defense Metals and Ceramics Information Center Battelle Memorial Institute 505 King Avenue Columbus, OH 43201	1
Metals and Ceramics Division Oak Ridge National Laboratory P.O. Box X Oak Ridge, TN 37380	1
Los Alamos Scientific Laboratory P.O. Box 1663 Los Alamos, NM 87544 ATTN: Report Librarian	1
Argonne National Laboratory Metallurgy Division P.O. Box 229 Lemont, IL 60439	1
Brookhaven National Laboratory Technical Information Division Upton, Long Island New York 11973 ATTN: Research Library	1
Office of Naval Research Branch Office 1030 East Green Street Pasadena, CA 91106	1

DISTRIBUTION LIST
Corrosion Mechanisms

Professor J. P. Hirth
Ohio State University
Department of Metallurgical Engineering
1314 Kinnear Road
Columbus, OH 43212

Dr. J. Kruger
National Bureau of Standards
Washington, DC 20234

Dr. H. K. Birnbaum
University of Illinois
Department of Metallurgy and Mining Engineering
Urbana, IL 61801

Dr. D. J. Duquette
Rensselaer Polytechnic Institute
Department of Metallurgical Engineering
Troy, NY 12181

Dr. R. P. Wei
Lehigh University
Institute for Fracture and Solid Mechanics
Bethlehem, PA 18015

Prof. H. W. Pickering
Pennsylvania State University
Department of Material Science
University Park, PA 16802

Prof. I. M. Bernstein
Carnegi-Mellon University
Schenley Park
Pittsburg, PA 15213

Dr. T. R. Beck
Electrochemical Technology Corporation
10035 31st Avenue, N.E.
Seattle, WA 98125

Prof. R. T. Foley
The American University
Washington, DC 20016

Dr. D. L. Davidson
Southwest Research Institute
8500 Culebra Road
P.O. Box Drawer 28510
San Antonio, TX 78284

Dr. Barry C. Syrett
Stanford Research Institute
333 Ravenswood Avenue
Menlo Park, CA 94025

Prof. S. Weissmann
Rutgers, The State University
of New Jersey
College of Engineering
New Brunswick, NY 08903

Prof. H. Herman
State University of New York
Material Science Department
Stony Brook, NY 11794

Prof. R. M. Latanision
Massachusetts Institute of
Technology
77 Massachusetts Avenue, Room E19-702
Cambridge, MA 02139

Prof. E. A Starke. Jr.
Dept. of Materials Science
University of Virginia
Charlottesville, VA 22901

Prof. Morris E. Fine
Northwestern University
The Technological Institute
Evanston, IL 60201

Dr. C. S. Kortovich
TRW, Inc.
2355 Euclid Avenue
Cleveland, OH 44117

Dr. O. Buck
Rockwell International Science Center
1049 Camino Dos Rios
P.O. Box 1085
Thousand Oaks, CA 91360

Dr. R. J. Arsenault
University of Maryland
College Park,MD 20742

Dr. F. Mansfeld
Rockwell International (Science Ctr)
1049 Camino Dos Rios
P.O. Box 1085
Thousand Oaks, CA 91360

Continue of Distribution List

036
16 November 1981

Dr. Paul Gordon
Illinois Institute of Technology
Department of Metallurgical and Materials
Engineering
Chicago, IL 60616

Dr. H. Leidheiser, Jr.
Lehigh University
Bethlehem, PA 18015

Dr. J. V. McArdle
University of Maryland
College Park, MD 20742

Br. E. McCafferty
Naval Research Laboratory
Washington, DC 20375

Prof. J. G. Byrne
The University of Utah
Dept. of Materials Science & Engineering
Salt Lake City, Utah 84112

Prof. A. J. Ardell
University of California
School of Engineering and Applied Science
405 Hilgard Ave.
Los Angeles, CA 90024

Prof. J. A. S. Green
Martin Marietta Corporation
1450 South Rolling Road
Baltimore, MD 21227

Prof. G.H. Meier & F.S. Pettit
University of Pittsburgh
Dept. of Matallurgical and Materials
Engineering
Pittsburgh, PA 15261

Prof. Alexander M. Cruickshank
Gordon Research Conference
Pastore Chemical Laboratory
University of Rhode Island
Kingston, RI 02881

Dr. Theordore R. Beck
Electrochemical Technology Corp.
3935 Leary Way NW
Seattle, Washington 98107

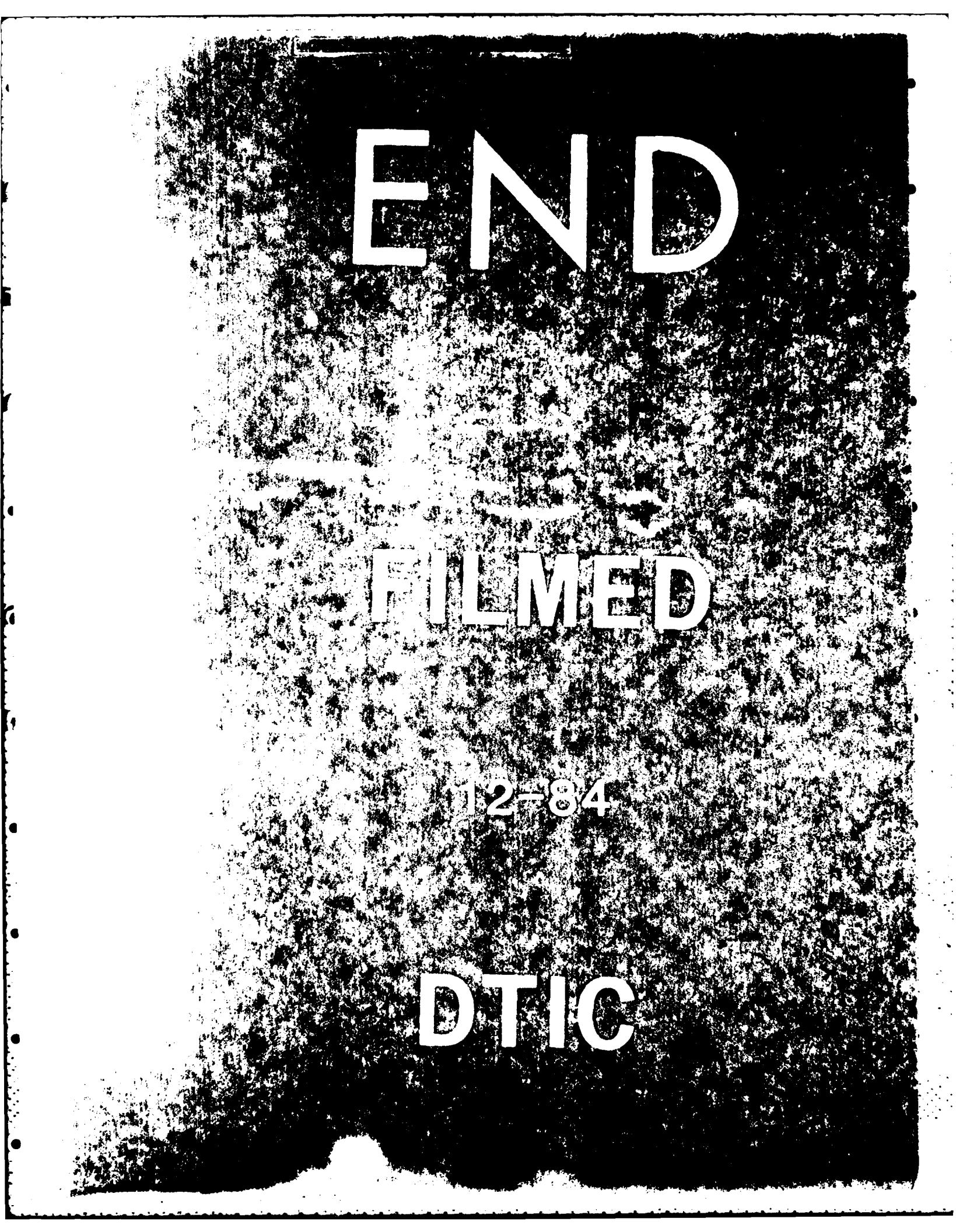
END
FILMED
12-84
DTIC